ADVANCES IN ATMOSPHERIC SCIENCES, VOL. 21, NO. 5, 2004, 755–766

# The Effect of Diapycnal Mixing on the Ventilation and CFC-11 Uptake in the Southern Ocean

Yongqi GAO*[1,2,3] and Helge DRANGE[1,2,3,4]

[1] *Nansen Environmental and Remote Sensing Center, Bergen, Norway*

[2] *Nansen-Zhu International Research Centre, Institute of Atmospheric Physics, Chinese Academy of Sciences, Beijing* 100029

[3] *Bjerknes Centre for Climate Research, Bergen, Norway*

[4] *Geophysical Institute, University of Bergen, Bergen, Norway*

(Received 19 November 2003; revised 4 March 2004)

**ABSTRACT**

The Miami Isopycnic Coordinate Ocean Model (MICOM) is used to investigate the effect of diapycnal mixing on the oceanic uptake of CFC-11 and the ventilation of the surface waters in the Southern Ocean (south of 45°S). Three model experiments are performed: one with a diapycnal mixing coefficient $K_{\rm d}$ ($\rm m^2\ s^{-1}$) of $2\times10^{-7}/N$ (Expt. 1), one with $K_{\rm d}=0$ (Expt. 2), and one with $K_{\rm d}=5\times10^{-8}/N$ (Expt. 3), $N$ ($\rm s^{-1}$) is the Brunt-Väisälä frequency. The model simulations indicate that the observed vertical distribution of CFC-11 along 88°W (prime meridian at 0°E) in the Southern Ocean is caused by local ventilation of the surface waters and westward-directed (eastward-directed) isopycnic transport and mixing from deeply ventilated waters in the Weddell Sea region. It is found that at the end of 1997, the simulated net ocean uptake of CFC-11 in Expt. 2 is 25% below that of Expt. 1. The decreased uptake of CFC-11 in the Southern Ocean accounts for 80% of this difference. Furthermore, Expts. 2 and 3 yield far more realistic vertical distributions of the ventilated CFC-waters than Expt. 1. The experiments clearly highlight the sensitivity of the Southern Ocean surface water ventilation to the distribution and thickness of the simulated mixed layer. It is argued that inclusion of CFCs in coupled climate models could be used as a test-bed for evaluating the decadal-scale ocean uptake of heat and $CO_2$.

**Key words:** chlorofluorocarbons, CFC-11, diapycnal mixing, ocean modelling, ocean ventilation, Southern Ocean, transient tracers

## 1. Introduction

Ocean General Circulation Models (OGCMs) are key tools in the assessment of the future ocean uptake of atmospheric greenhouse gases and heat. Furthermore, whereas nature experiences one realisation of the climate state, climate models can be used as a laboratory to produce a multitude of climate realisations, and by that contribute to the understanding of the variability and stability properties of the system. It is, in this respect, crucial to evaluate the climate models against observed quantities to assess the degree of realism of the models.

Numerical simulations with OGCMs indicate that the Southern Ocean is the largest sink of human-induced $CO_2$ in the World Oceans (Orr et al., 2001), and that the simulated tracer distributions vary significantly between different models (Dutay et al., 2002.) Recent studies show that the vertical or, in the isopycnic frame work, the diapycnal mixing plays a key role in the ventilation of the Southern Ocean (Robitaille and Weaver, 1995; Sloyan and Rintoul, 2000). It is therefore interesting to test the effect of diapycnal mixing on the ventilation of the surface waters, and consequently on the ocean uptake and storage of greenhouse gases and heat.

Chlorofluorocarbons CFC-11 ($CCl_3F$) and CFC-12 ($CCl_2F_2$) were introduced to the atmosphere in the early 1930s, and their atmospheric evolution (Fig. 1) is fairly well known. CFCs are man-made and are chemically and biologically inactive in the ocean, and are therefore well suited to evaluate ocean ventilation

*E-mail: yong@nersc.no

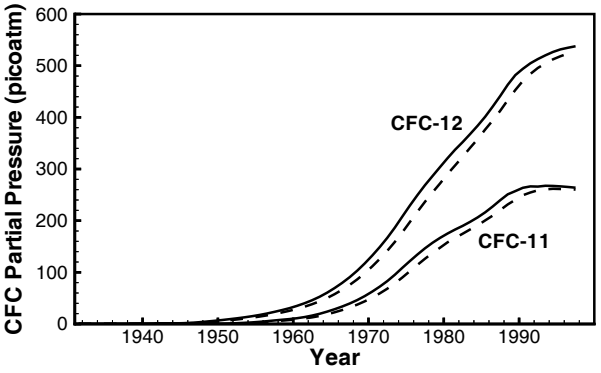


**Fig. 1.** Reconstructed history of the partial pressure of CFC-11 and CFC-12 in dry air at one atmosphere pressure (Walker et al., 2000). The solid (dashed) line corresponds to the CFC concentrations in the Northern (Southern) Hemisphere.

processes on interannual to decadal timescales. The recent World Ocean Circulation Experiment (WOCE) has conducted global surveys of the distributions of the CFCs (see http://whpo.ucsd.edu/distmaps.htm). Furthermore, numerical studies have demonstrated that validation against observed distributions of CFCs is a powerful method to explore mixing and transport properties in OGCMs (Dixon et al., 1996; Dutay et al., 2002; Beismann and Redler, 2003; Gao et al., 2003) and to infer sources and mixing pathways of water masses in general (Orsit et al., 2002; Smethie Jr et al., 2000).

The objective of this study is to explore the ventilation processes in the Southern Ocean, hereafter defined as the region between 45°S and 69°S, by an isopycnic-coordinate OGCM. For this, the observed CFC-11 distributions along WOCE section P19 at 88°W during 1993 (Willey et al., 2004) and along the Ajax section at the prime meridian during early 1984 (Warner and Weiss, 1992) have been compared with the simulated CFC-11 distributions along the same sections.

Model-data evaluations are, in general, based on classical geopotential (or $z$-coordinate) OGCMs. The newly developed isopycnic coordinate OGCMs (e.g., Bleck et al., 1992; Oberhuber, 1993) have the advantage that mixing across the coordinate interfaces can be exactly represented for a given value of the diapycnal mixing coefficient $K_\mathrm{d}$. In the configuration $K_\mathrm{d} = 0$, the coordinate interfaces are material surfaces, and thereby truly isolate the effect of transport and mixing along the coordinate layers. The latter property is intriguing for the ocean environment, as the preferred plane of flow and mixing is along, rather than across, planes of constant density (Ledwell and Watson, 1993; Toole et al., 1994).

## 2. Model description and experimental design

### 2.1 *Model description and configuration*

The OGCM used in this study is the Miami Isopycnic Coordinate Ocean Model (MICOM; Bleck et al., 1992). MICOM is a primitive equation model utilizing surfaces of constant density as the vertical coordinate. In the present study, potential density at $2\times10^7$ Pa ($\sigma_2$) is used as the reference level for the vertical coordinate surfaces.

The modeled ocean consists of a surface mixed layer in which the potential density varies in time and space, and 15 interior isopycnic layers. For the mixed layer, the Gaspar (1998) bulk-parameterization is used. All the air-sea exchanges of momentum, heat, and freshwater are incorporated into the mixed layer using conventional bulk formulae. No surface restorations of SST or sea surface salinity (SSS) are applied. Convective mixing takes place if the density of the mixed layer exceeds the density of one or more of the underlying isopycnals. The instability is then removed by mixing all of the unstable water masses, and by absorbing the new water mass into the mixed layer. Both momentum and tracers are uniformly mixed in the case of convective mixing.

The interior isopycnals exchange their properties with the mixed layer if they outcrop to the mixed layer. Therefore, the location and timing of the outcropping of the isopycnic layers are of crucial importance in analyzing the ocean ventilation of any of the mixed layer properties. In addition, mixing is prescribed in the direction normal to the isopycnic interfaces. The associated diapycnal mixing coefficient $K_\mathrm{d}$ ($\mathrm{m^2\ s^{-1}}$) is proportional to $N^{-1}$ (Gargett, 1984), where

$$N = \sqrt{\frac{g}{\rho}\frac{\partial\rho}{\partial z}} \qquad (\mathrm{s^{-1}})$$

is the Brunt-Väisälä frequency, $g$ ($\mathrm{m\ s^{-2}}$) is the gravitational acceleration, $\rho$ ($\mathrm{kg\ m^{-3}}$) is the density, and $z$ (m) is the depth. For the base-line integration (Expt. 1 in the following), the proportionality coefficient is set to $2\times10^{-7}$ $\mathrm{m^2\ s^{-2}}$. The numerical implementation of the diapycnal mixing follows the scheme of McDougall and Dewar (1998). Readers interested in the intrinsic model features are referred to Bleck et al. (1992).

The setup of the applied version MICOM follows Sun (1997). The model domain spans the region from 65°N to 69°S. No temperature and salinity relaxation are applied at the northern and southern boundaries of the model domain. At the northern boundary, a prescribed flow of 6 Sv in layer 13 ($\sigma_2 = 37.11$) mimics the outflow from the Nordic Seas, whereas a prescribed flow of 3 Sv originates from the Weddell Sea in layer 15

($\sigma_2 = 37.17$). A regular grid on a Mercator projection is used and a rather coarse latitude-by-longitude resolution of $2^\circ \times 2^\circ \cos\phi$ (where $\phi$ is latitude) is chosen for the experiments. The $\sigma_2$ values for the isopycnic layers are 33.22, 34.26, 35.04, 35.62, 36.05, 36.37, 36.61, 36.79, 36.92, 37.01, 37.07, 37.11, 37.14, 37.17, and 37.20, and then the equations are differentiated on an Arakawa and Lamb (1977) C-grid stencil.

The diffusive velocities (diffusivities divided by the size of the grid cell) for layer interface diffusion, momentum dissipation, and temperature/salinity mixing are 0.005 m s$^{-1}$, 0.01 m s$^{-1}$, and 0.005 m s$^{-1}$ respectively, yielding actual diffusivities on the order of $10^3$ m$^2$ s$^{-1}$ for a 100-km grid spacing. The presence of sea ice has been mimicked by setting the surface wind stirring and the heat fluxes to zero wherever the modeled mixed layer temperature is below $-1.8^\circ$C. No ice-related physical processes, for instance brine rejection (Anderson and Jones, 1991), are incorporated in the model.

Atmospheric surface forcings applied to the model include monthly mean climatological surface wind stress, atmospheric relative humidity and surface temperature from the Comprehensive Oceanographic and Atmospheric Data Set (COADS; Woodruff et al., 1987). The monthly mean climatological net radiation flux is from the Oberhuber (1988) Atlas, and the precipitation is from the NOAA microwave sunder (Spencer, 1993).

The model was initialized by the Levitus and Boyer (1994) and Levitus et al. (1994) January climatological temperature and salinity fields, respectively, and with the ocean at rest.

Following the atmospheric record (Fig. 1), the CFC simulation starts in 1931 with a zero CFC concentration in the atmosphere and the ocean. The fluxes of CFCs at the air-sea surface are expressed as:

$$F = K_{\mathrm{w}} \cdot (C_{\mathrm{sat}} - C_{\mathrm{surf}}), \qquad (1)$$

where $F$ (mol m$^{-2}$ s$^{-1}$) is the flux of the CFCs, $C_{\mathrm{sat}}$ (mol m$^{-3}$) is the temperature-and salinity-dependent saturated CFC concentration at the sea surface, $K_{\mathrm{w}}$ (m s$^{-1}$) is the wind dependent transfer (or piston) velocity, and $C_{\mathrm{surf}}$ (mol m$^{-3}$) is the modeled surface ocean CFCs concentration. The transfer velocity $K_{\mathrm{w}}$ is computed using Eq. (3) in Wanninkhof (1992) with wind speed from the first and second Special Sensor Microwave Imager (SSMI) satellite data prepared as described in Boutin and Etcheto (1997) and Orr et al. (2001). For details about introducing CFCs into OGCMs, please refer to the description in Dutay et al. (2002).

### 2.2 *Model experiments*

The OGCM was first spun up for 164 years with $K_{\mathrm{d}} = 2 \times 10^{-7}/N$. Thereafter, three on-line CFC simulations were conducted for the period 1931 to 1997 (see Table 1). It should be noted that Expt. 1 is identical to the NERSC (Nansen Environmental and Remote Sensing Center) model version used in the model intercomparison paper of Dutay et al. (2002). In the latter study, it was found that the NERSC model strongly overestimated the ocean uptake of CFC-11. Experiments 2 and 3 therefore address a potential reason for the model deficiency pointed out in Dutay et al. (2002).

The value of $K_{\mathrm{d}}$ in Expt. 1 is identical to a recently estimated value of $K_{\mathrm{d}}$ in the pycnocline over the South Scotia Ridge at the northwestern entrance of the Weddell Sea (Muench et al., 2002). Since, for instance, tidal dissipation is expected to be particularly strong over rough topography (e.g., Ledwell et al., 2000; Muench et al., 2002), it is expected that Expt. 1 represents an upper (but realistic) bound on $K_{\mathrm{d}}$. The model sensitivity to $K_{\mathrm{d}}$ is bracketed by Expt. 2, whereas Expt. 3 represents an intermediate value of $K_{\mathrm{d}}$.

The main motivation for the experimental setup is, as already described, to fully exploit the isopycnal versus diapycnal influence on the ventilation of the Southern Ocean waters. It should be stressed that the experiments should be viewed as sensitivity experiments as the spin-up integration is similar for all of the experiments. The use of identical initial conditions for the physical model imply that the isolated effect of isopycnal versus diapycnal transport and mixing is more transparent than for the case with three independent model spinups. A more realistic model configuration would include fully independent model integrations (i.e., three separate model spinups), the use of realistic (i.e., synoptic) atmospheric forcing fields, and a truly global model domain including a full dynamic-thermodynamic sea ice module. Results from the latter approach for the Atlantic Ocean are presented in Gao et al. (2003).

## 3. Results

### 3.1 *Ocean storage and uptake of CFC-11*

The simulated ocean inventory of CFC-11 is provided in Fig. 2. At the end of 1997, the CFC-11 inventory is $820 \times 10^6$ mol in Expt. 1 and $614 \times 10^6$ mol

**Table 1.** Diapycnal diffusivities $K_{\mathrm{d}}$ (m$^2$ s$^{-1}$) applied in the CFC simulations.

| Expt. 1 | Expt. 2 | Expt. 3 |
|---|---|---|
| $2 \times 10^{-7}/N$ | 0 | $5 \times 10^{-8}/N$ |

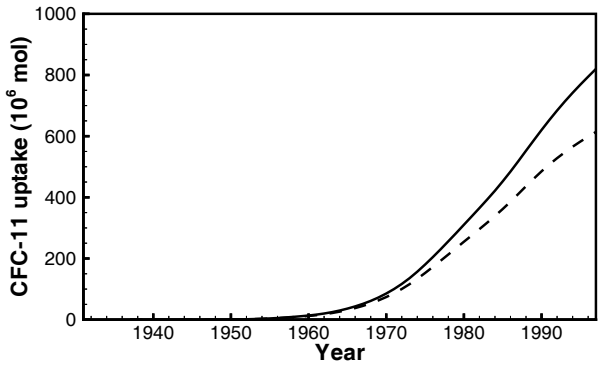


**Fig. 2.** Time evolution of the simulated oceanic uptake of CFC-11 ($10^6$ mol) in Expt. 1 (solid line) and Expt. 2 (dashed line).

in Expt. 2, or 75% of that of Expt. 1. These figures clearly indicate the model dependency on $K_{\rm d}$.

The zonally integrated inventory and the accumulated flux of CFC-11 (Fig. 3) illustrate that by far the most efficient uptake and storage of CFC-11 take place in the Southern Ocean. The shift between the accumulated CFC-fluxes at about 60°S and the maximum inventories at about 45°S shows the equatorward transport of CFC-11 from the high southern latitudes.

The accumulated CFC-11 flux in the Southern Ocean can be deduced from Fig. 3. The obtained values are about $475\times10^6$ mol for Expt. 1 and $311\times10^6$ mol for Expt. 2, accounting for as much as 58% and 50% of the simulated World Ocean uptake, respectively. Furthermore, the difference in the Southern Ocean's uptake between the two experiments, $164\times10^6$ mol, accounts for 80% of the total difference of $206\times10^6$ mol between the two experiments, despite the fact that the area of the Southern Ocean is only about 30% of the model domain. Finally, the average accumulated CFC-11 fluxes in the Southern Ocean are $8.63\times10^{-6}$ mol m$^{-2}$ and $5.65\times10^{-6}$ mol m$^{-2}$ in Expts. 1 and 2, respectively, yielding a difference of 35%.

### 3.2 *The meridional distribution of CFC-11*

To qualitatively illustrate the reason for the difference in the meridional distribution of the CFC-11 fluxes, Eq. (1) can be expressed as follows:

$$F = K_{\rm w}\cdot C_{\rm sat}\cdot\left(1-\frac{C_{\rm surf}}{C_{\rm sat}}\right) = K_{\rm w}\cdot C_{\rm sat}\cdot(1-P_{\rm surf})\,, \quad (2)$$

where $P_{\rm surf}$ is the saturation degree of the CFCs. The above expression yields the flux $F$ grid point by grid point. To simplify the analyses, a virtual flux $F_{\rm v}$ (mol m$^{-2}$ s$^{-1}$) can be defined as:

$$F_{\rm v} = \overline{K_{\rm w}}\cdot\overline{C_{\rm sat}}\cdot\left[1-\overline{\left(\frac{C_{\rm surf}}{C_{\rm sat}}\right)}\right] = \overline{K_{\rm w}}\cdot\overline{C_{\rm sat}}\cdot\left(1-\overline{P_{\rm surf}}\right)\,, \quad (3)$$

where the overbar denotes the zonal average.

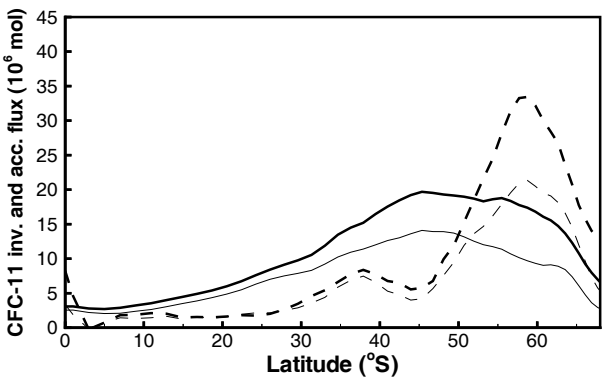


**Fig. 3.** Zonally integrated inventories of CFC-11 ($10^6$ mol) (solid lines) and accumulated flux of CFC-11 ($10^6$ mol) (dashed lines) at the end of 1997. Experiment 1 in thick lines and Expt. 2 in thin lines.

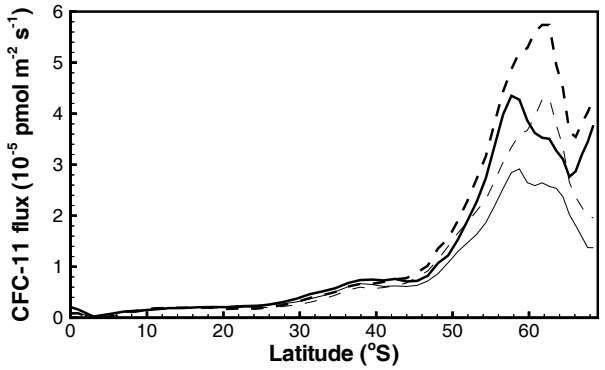


**Fig. 4.** Zonally averaged CFC-11 flux $\overline{F}$ (solid lines) and virtual flux $F_{\rm v}$ (dashed lines) ($10^{-5}$ pmol m$^{-2}$ s$^{-1}$) in September 1990. Expt. 1 in thick lines and Expt. 2 in thin lines.

In the experiments, the maximum uptake of CFC-11 in the Southen Ocean takes place in September, when the mixed layer temperature is low and subsequently the mixed layer is deep (see below). The zonally averaged CFC-11 flux obtained by zonally averaging $F$ in Eq. (2) and the virtual flux $F_{\rm v}$ from Eq. (3) are depicted in Fig. 4 for Expts. 1 and 2 for September 1990. In both experiments, the meridional variations in $F_{\rm v}$ follow, in general, those of $\overline{F}$. Therefore, the factors governing the meridional variation in the virtual flux $F_{\rm v}$, rather than the grid point flux $F$, are addressed next.

Figure 5 shows the simulated zonal mean CFC-11 saturation degree and the mixed layer salinity and thickness in September 1990 for Expts. 1 and 2. The surface CFC-11 concentration is significantly undersaturated in the Southern Ocean (Fig. 5a) implying that the Southern Ocean acts as a sink of CFC-11. The saturation degree is about 95% from 10°S to 40°S and decreases south of 45°S. At the southern boundary, the saturation degree is about 52% and 80% in Expts. 1 and 2, respectively.

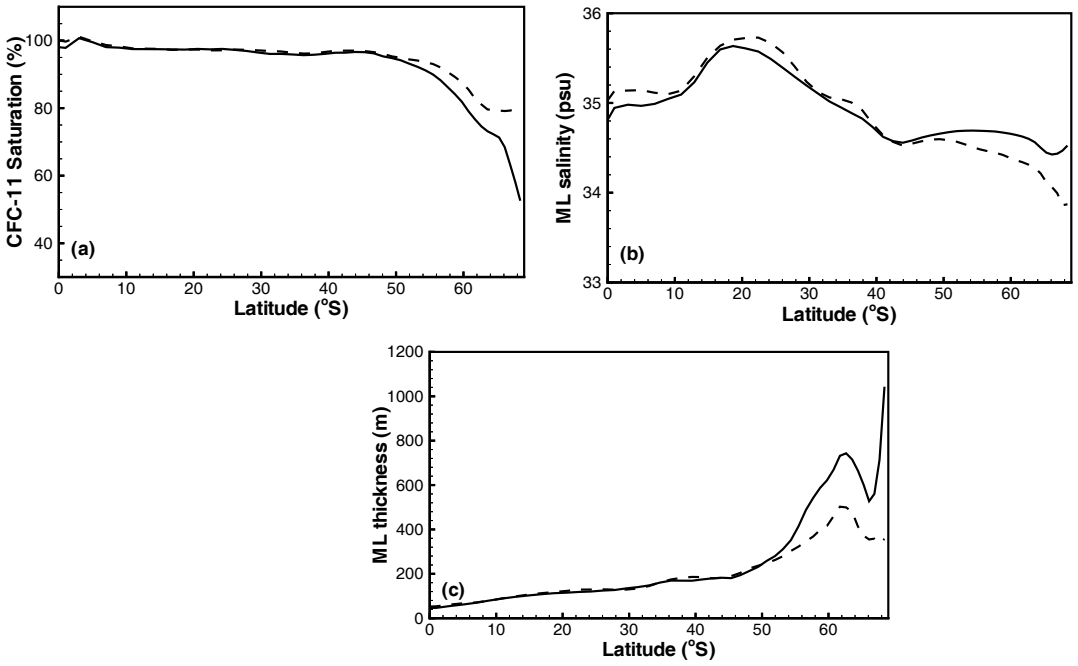


**Fig. 5.** Simulated zonal mean CFC-11 saturation degree (a), mixed layer salinity (b) (units: psu) and mixed layer thickness (c) (units: m) in September 1990. The solid (dashed) lines represent Expt. 1 (Expt. 2).

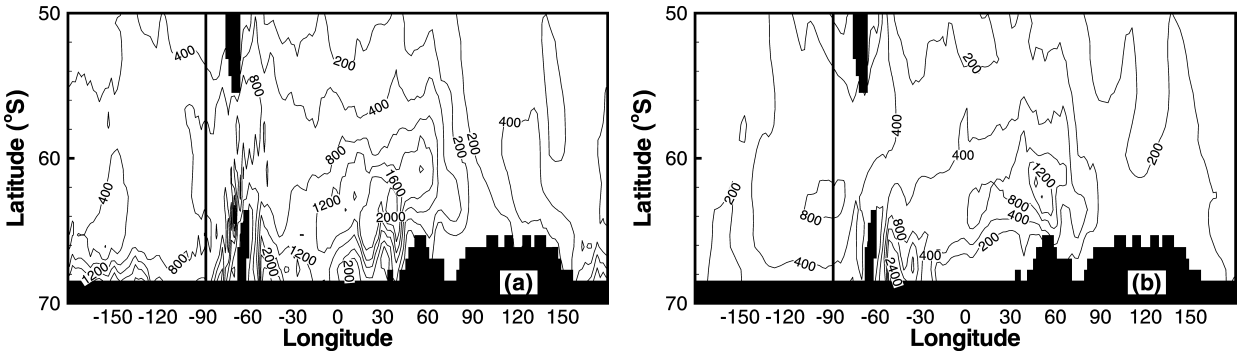


**Fig. 6.** Simulated maximum mixed layer thickness (m) in the Southern Ocean in Expt. 1 (a) and Expt. 2 (b) in year 1990. Shaded areas denote mixed layer > 800 m, and the WOCE P19 section is marked at 88°W.

The potential temperature is essentially identical in Expts. 1 and 2, yielding very similar CFC-11 saturation concentrations. The salinity, however, is significantly higher in Expt. 1 poleward of 45°S (Fig. 5b). Therefore, the mixed layer extends deeper in Expt. 1 than in Expt. 2 (Fig. 5c). The latter is of importance for the ocean uptake of the CFCs, as a deep mixed layer implies a volumetric dilution of the mixed layer CFC-11 concentration and consequently a prolonged air-sea equilibration time, and by that an enhanced ocean uptake, of the CFCs.

### 3.3 *Ventilation of the Southern Ocean*

The simulated mixed layer thickness and the locations of the outcroping isopycnals are key quantities in assessing the ventilation of the different water masses. In Expt. 2, the mixed layer water is the only source for the ventilation of the sub-surface water masses due to

the vanishing diapycnal mixing.

The simulated maximum mixed layer thickness distribution in the Southern Ocean is displayed in Fig. 6 for Expts. 1 and 2. In Expt. 1, surface mixing reaches a depth of 2400 m in the Weddell Sea (45°W), 1200 m along the southern boundary in the Pacific Ocean sector, and more than 1600 m between 62°S and 66°S in the Indian Ocean sector (10°–60°E). As a result, the penetration depth of the CFC-11 signal will be large in the areas where the simulated deep mixing occurs. In Expt. 2, the simulated deep convection in the Weddell Sea is similar with that in Expt. 1. However, convective mixing reaches only 400 m along the southern boundary in the Pacific Ocean sector and 800-1600 m in the Indian Ocean sector. As a result, CFC-11 does not, in general, penetrate as deep in Expt. 2 as in Expt. 1.

The location of the outcropping isopycnals determines the source waters of the interior model ocean. To illustrate this, the density of the outcroping isopycnals in September, the month of maximum mixed layer thickness, is displayed in Fig. 7. In Expts. 1 and 2, the 37.17 isopycnal outcrops to the surface in the Weddell Sea, and will consequently be ventilated by the properties of the mixed layer waters in this region. An additional source for the ventilation of the near bottom $\sigma_2 \geqslant 37.17$ isopycnals in Expt. 1 is located west of the Antarctic Peninsula where the 37.17 isopycnal outcrops to the surface. Therefore, the source for the ventilation of the 37.17 isopycnal will be the Weddell Sea and west of the Antarctic Peninsula in Expt. 1, and the Weddell Sea only in Expt. 2.

In the Pacific sector of the Southern Ocean in Expt. 1, the 37.14 isopycnal outcrops to the surface in the Ross Sea (at about 180°E) whereas the 37.11 isopycnal outcrops to the surface along most of the southern boundary. For comparison, no dense water masses with $\sigma_2 > 36.92$ outcrops to the surface between 90°E and 80°W in Expt. 2. Therefore, the presence of CFC-11 in waters with $\sigma_2 > 36.92$ in Expt. 2 can only be attributed to isopycnal transport and dispersive mixing from the source region east of 80°W and west of 90°E. West of the Antarctic Peninsula, the 37.14 isopycnal outcrops to the surface in Expt. 2. In the Indian sector, the 37.11 isopycnal outcrops to the surface between 64°S and 66°S in Expt. 1, whereas it is the 37.07 isopycnal that outcrops to the surface in the similar area in Expt. 2.

To illustrate the meridional difference in the distribution of CFC-11, the observed and the simulated CFC-11 concentrations along the WOCE P19 section at 88°W (Willey et al., 2004) are given in Fig. 8. At the surface, the largest differences are seen north of 10°S with too strong mixing in Expt. 1, too weak mixing in Expt. 2, and a fairly realistic mixing in Expt. 3. However, substantial differences are clearly seen in the distribution of CFC-11 in the bulk part of the intermediate and deep waters of the Southern Ocean. In Expt. 1, the simulated invasion of CFC-11 is far deeper and more widespread than in the observations (see also Fig. 10 in Dutay et al., 2002). In fact, there is almost no CFC-11 signal between 2400 m and 2600 m in the observations. This is in contrast to Expt. 1 where CFC-11 penetrates to the bottom at all latitudes south of 45°S. The vertical distribution is, however, greatly improved in Expts. 2 and 3.

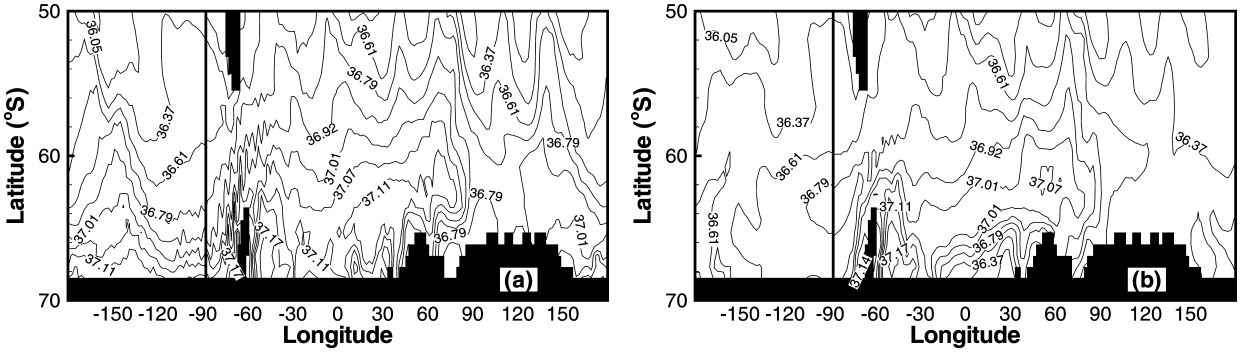


**Fig. 7.** Locations of the outcroping isopycnals when the mixed layer is at maximum state in 1990 in Expt. 1 (a) and Expt. 2 (b). The shaded areas denote where the $\sigma_2 \geqslant 37.11$ isopycnals outcrop to the surface. The WOCE P19 section is shown at 88°W.

To quantitatively evaluate the ocean storage of CFC-11, the simulated and observed inventory along the P19 section are shown in Fig. 9. All the simulations overestimate the CFC-11 inventory south of 60°S in the Southern Ocean by a factor of 2 or more, and particularly Expt. 1. Furthermore, the CFC-11 inventory decreases with reduced strength of the diapycnal mixing, as expected.

To investigate the reason for the differences in the distribution of the observed and simulated CFC-11 concentrations along the WOCE P19 section, the climatological and the simulated density stratifications are shown in Fig. 10. In Expt. 1, the simulated deep convection reaches 1200 m south of 66°S, and here the 37.11 isopycnal outcrops to the mixed layer. Therefore, by water mass transfer, the 37.11 isopycnal will be ventilated by the mixed layer water and the CFC-11 signal will be entrained onto the layer. It also follows from the figure that the 37.17 isopycnal is not ventilated by the mixed layer water locally. Therefore, the presence of CFC-11 on the 37.17 isopycnal along the WOCE P19 section (c.f., Fig. 8b) is caused by isopycnal transport and dispersive mixing from other locations in the Southern Ocean. In Expt. 2, the simulated mixed layer thickness is about 500 m at the southern boundary, and here the 37.01 isopycnal outcrops to the surface. Therefore, the 37.01 isopycnal can be ventilated by the mixed layer water at 88°W. Clearly, the 37.11, 37.14, and 37.17 isopycnals cannot be ventilated by mixed layer water locally. The presence of CFC-11 on these layers (c.f., Fig. 8c) is therefore a result of isopycnal transport and mixing. The situation for Expt. 3 falls between Expts. 1 and 2, but is closest to Expt. 2.

It should be noted that the simulated deep convection south of 60°S is stronger in all of the experiments than that inferred from the climatological density stratification. The overestimated mixing depth forces the deepest isopycnals to outcrop to the surface and will surely result in the overestimated CFC-11 uptake by the model, in accordance with Fig. 9.

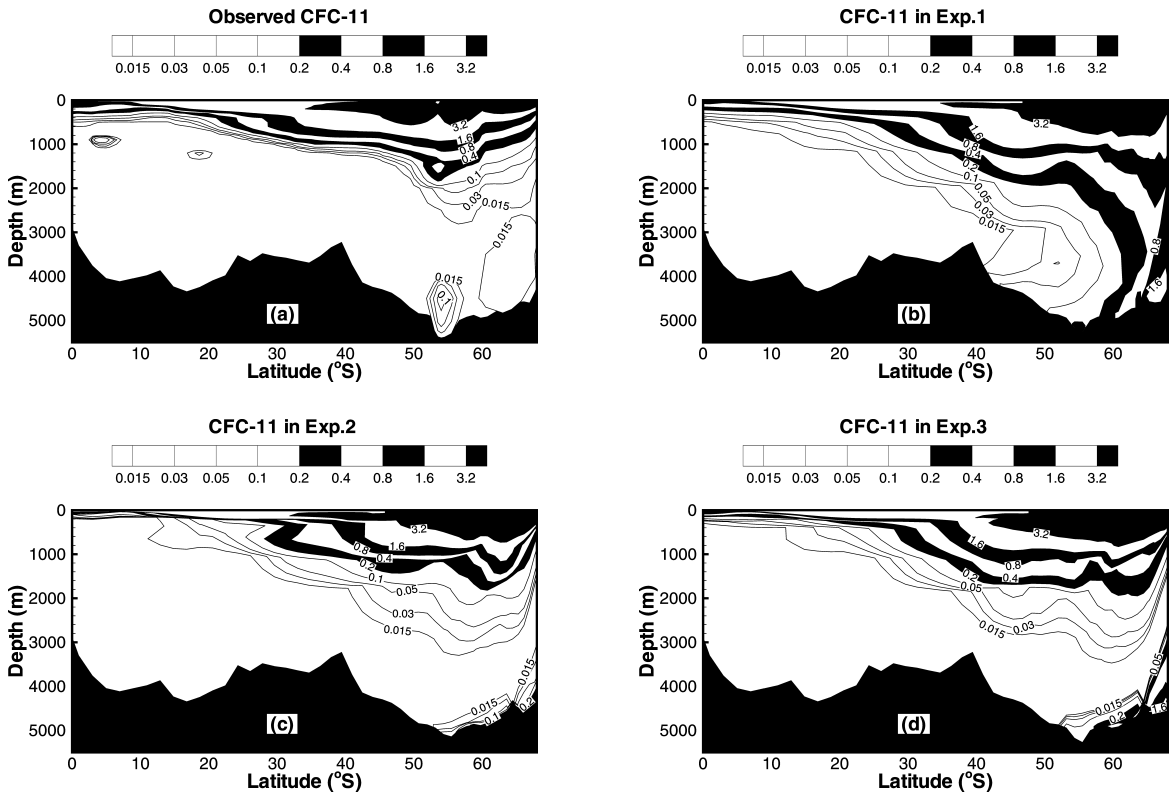


**Fig. 8.** Observed (a) and simulated (b–d) CFC-11 (pmol $kg^{-1}$) along WOCE P19 section at 88°W in the Southern Pacific in early 1993. The cut-off value of the CFC-11 concentration is 0.01 pmol $kg^{-1}$ in all panels. Observed CFC-11 from P19c and P19s is available from http://whpo.ucsd.edu/data/onetime/pacfic/p19/.

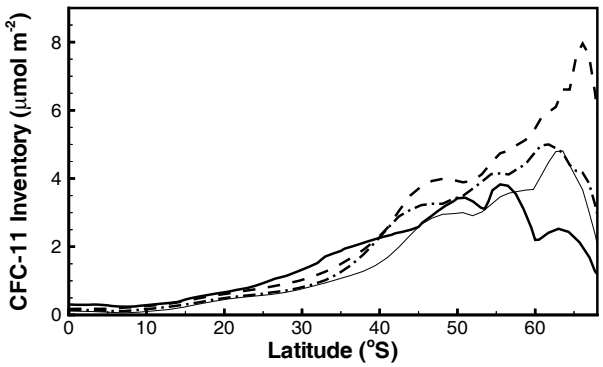


**Fig. 9.** Observed and simulated CFC-11 inventories ($\mu$mol m$^{-2}$) along WOCE P19. The thick solid line, the dashed line, the thin solid line, and the dash-dotted line represent the inventories of CFC-11 in the observation, and in Expts. 1–3, respectively.

To further explore the model performance in the Southern Ocean, the observed and simulated CFC-11 distributions along the 1983–1984 Ajax section (Warner and Weiss, 1992) at the prime meridian in the South Atlantic Ocean are compared (Fig. 11). Similar comparisons are provided in Dutay et al. (2002) and Doney and Hecht (2002). In the observations, the vertical penetration of the CFC-11 signal down to about 1000 m deep between 55°S and 40°S indicates the formation of the Subantarctic Mode Water (SAMW). The weakly ventilated Circumpolar Deep Water is embodied by the low CFC concentration below SAMW. Close to the bottom, water with a relatively high concentration of CFC-11 represents the recently ventilated Antarctic Bottom Water. As illustrated by Orsi et al. (1999), the AABW in the Ajax section originates from the Weddell Sea.

The simulated CFC-11 along the Ajax section differs greatly in the experiments. The simulated sea surface CFC-11 concentrations are close to the observed values in Expt. 1, whereas Expts. 2 and 3 show too low mixing intensity in the surface waters north of 25°S. All experiments capture the sharp subsurface penetration of the CFC-11 associated with the ventilation of SAMW. However, the simulated ventilation south of 50°S is much stronger than in the observations, with the results from Expts. 2 and 3 being closest to the observed one.

To identify the source regions for the ventilation of the 37.17 isopycnal in Expts. 1 and 2, the isopycnal distribution of CFC-11 is displayed in Fig. 13. The CFC-11 distribution clearly indicates that the source of the ventilation is located in the Weddell Sea, the Ross Sea, and west of the Antarctic Peninsula in Expt. 1. In Expt. 2, the ventilation is located in the Weddell Sea and to some extent west of the Antarctic Peninsula. Therefore, the presence of CFC-11 at the bottom along the WOCE P19 section at 88°W and that along the Ajax section at the prime meridian are caused by isopycnal transport and mixing from east and west, respectively.

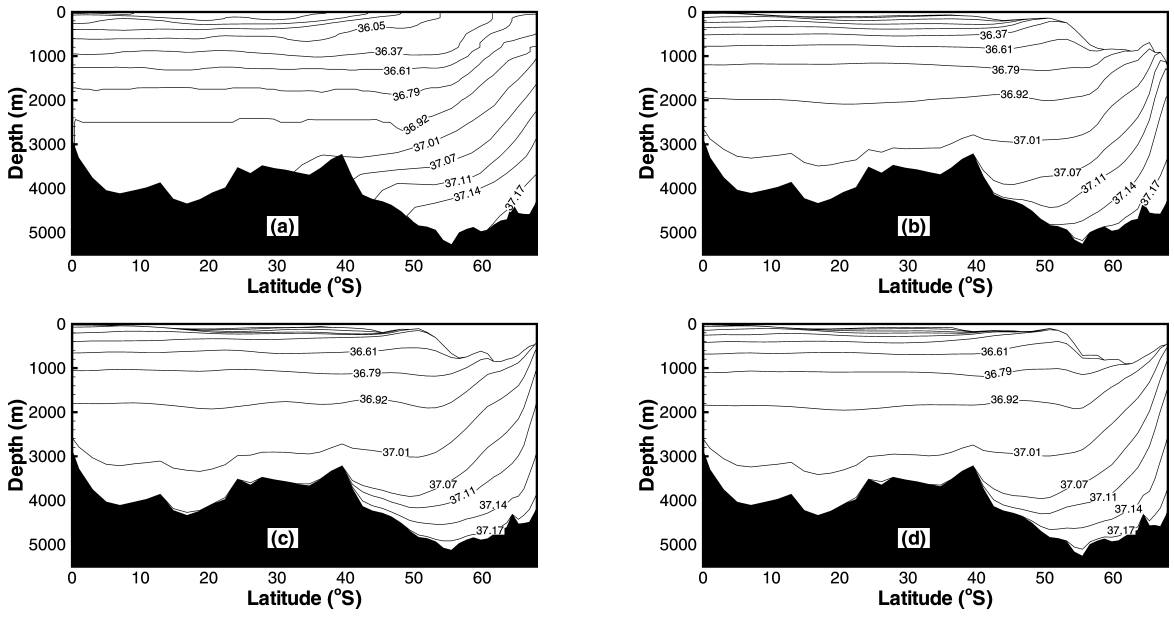


**Fig. 10.** Vertical distributions of (a) September climatological isopycnals from Levitus and Boyer (1994) and Levitus et al. (1994), and (b, c, d) simulated isopycnals in September of CFC-11 year 1993 in Expts. 1–3 along the WOCE P19 section.

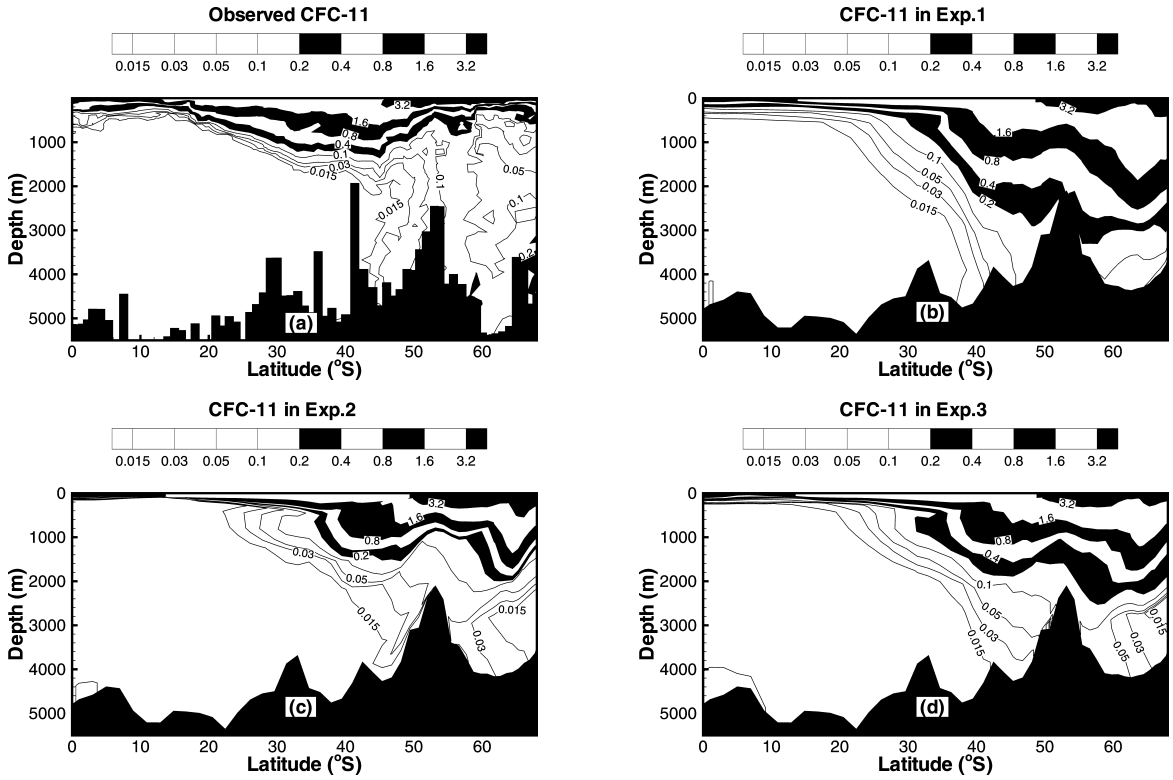


**Fig. 11.** Observed (a) and simulated (b–d) CFC-11 (pmol kg$^{-1}$) along the Ajax section along the prime meridian in early 1984 (Weiss et al.,1990; Warner and Weiss, 1992). The cut-off value of the CFC-11 concentration is 0.01 pmol kg$^{-1}$ in all panels. Observed CFC-11 from the Ajax section is available from http://www.ipsl.jussieu.fr/OCMIP/.

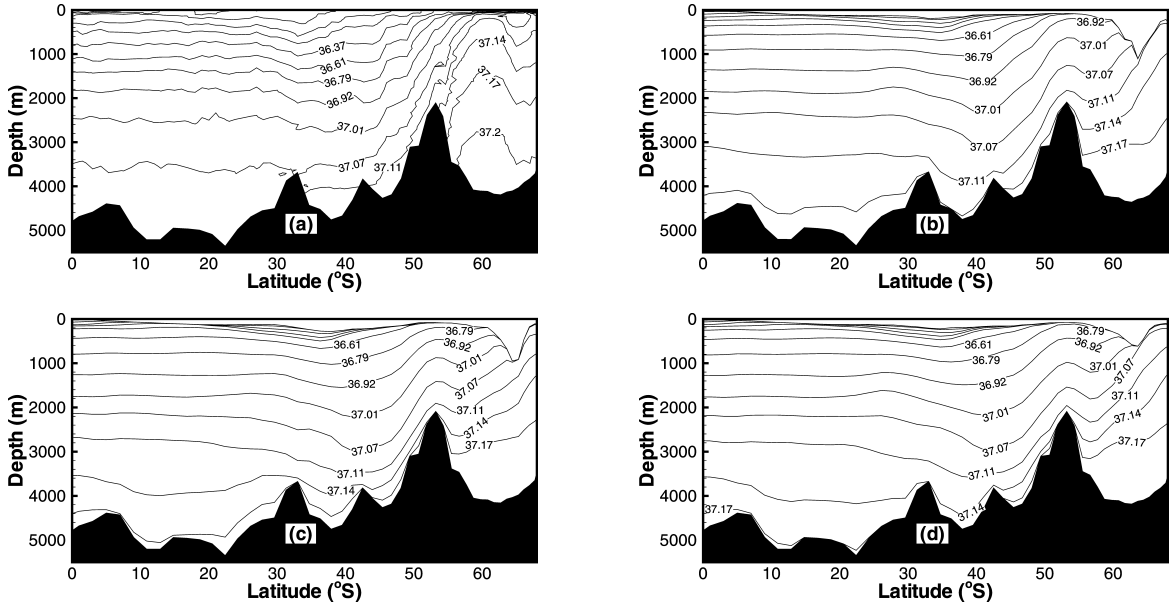


**Fig. 12.** Vertical distributions of (a) September climatological isopycnals from Levitus and Boyer (1994) and Levitus et al. (1994), and (b–d) simulated isopycnals in September of CFC-11 year 1983 in Expts. 1–3 along the Ajax (prime median) section.

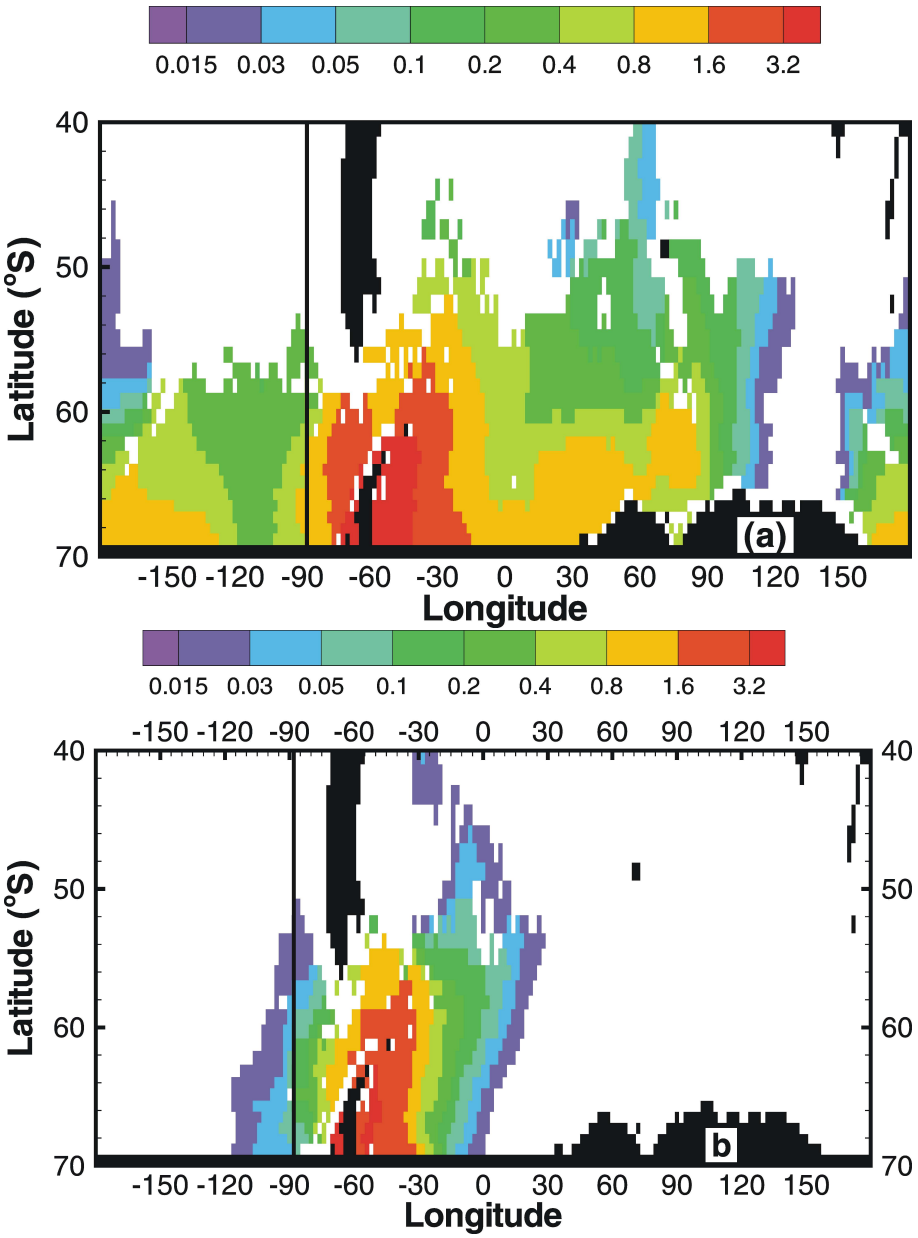


**Fig. 13.** Simulated CFC-11 (pmol kg$^{-1}$) on the 37.17 isopycnal in (a) Expt. 1 and (b) Expt. 2. Cut-off value is 0.01 pmol kg$^{-1}$. The WOCE P19 section is shown at 88°W.

## 4. Discussion and Conclusion

The sensitivity of the diapycnal mixing on the oceanic uptake of anthropogenic CFC-11 and the ventilation in the Southern Ocean have been investigated with a near global isopycnic coordinate ocean model. Three simulations have been conducted with diapycnal mixing coefficients of $K_d = 2 \times 10^{-7}/N$ (Expt. 1), $K_d = 0$ (Expt. 2), and $K_d = 5 \times 10^{-8}/N$ (Expt. 3). In Expt. 2, the transport and mixing of all of the model variables occur along the isopycnal layers as the isopycnic interfaces are truly material surfaces for vanishing $K_d$.

The model simulations indicate that the observed vertical distribution of CFC-11 along 88°W (Fig. 8) and along the prime meridian (Fig. 11) are caused by two processes: (1) local ventilation of the mixed layer waters leading to elevated CFC-11 concentrations over the uppermost 1000-2000 m of the water column, and (2) respectively westward (eastward) directed isopycnic transport and mixing from deeply ventilated waters in the Weddell Sea region.

In the model, the deepest ventilation takes place as convective mixing to a depth of more than 2000 m in the Weddell Sea (Fig. 6b) with subsequent transport and mixing along downward-sloping isopycnals (Figs. 10c and 13b), yielding CFC-11 signals in the bottom waters of the Southern Ocean north to about 55°S. The simulated and observed CFC-11 distributions show the same large-scale features (see Figs. 8a and 8c), although the CFC-enriched bottom water in the observation is possibly a result of a combination of deep convective mixing in the Weddell Sea and geostrophically-driven density currents formed under the Weddell Sea ice cap and subsequent turbulent mixing (e.g., Killworth, 1977).

The presented model experiments clearly show that the uptake of CFC-11 in the Southern Ocean and the subsequent spreading of the CFC-enriched water masses are sensitive to the applied diapycnal mixing. In fact, at the end of 1997, the simulated net ocean uptake of CFC-11 in Expt. 2 is 25% below that of Expt. 1. Of this reduction, the decreased uptake of CFC-11 in the Southern Ocean accounts for 80% of the total difference. It is further shown that weak and even vanishing diapycnal mixing greatly improves the simulated CFC-11 distribution in the Southern Ocean. Apparently, Expt. 3 with $K_{\mathrm{d}} = 5 \times 10^{-8}/N$ produced a vertical CFC-11 distribution that resembles the observed distribution quite well. The presented sensitivity experiments provide a plausible explanation to the overly diffusive characteristics of the NERSC model presented in the study of Dutay et al. (2002).

The experiments also highlight the sensitivity of the Southern Ocean mixed layer to the ventilation of the ocean interior. Rather small differences in the maximum mixed layer depth may easily generate huge differences in the time-space properties of the ventilated waters. One of the major challenges in climate modeling is therefore to simulate the ventilation of the Southern Ocean in a realistic manner to avoid, for instance, excessive ocean uptake of heat and $CO_2$. This is a tremendous challenge for coupled atmosphere-sea ice-ocean models as proper representation of the mixed layer dynamics in the region depends on the surface buoyancy (i.e., the heat and fresh water) and momentum forcing, the presence and the actual simulated seasonal cycle of sea ice including brine release, and the detachment of icebergs from the massive Antarctic ice shelves and Antarctic melt water in general. A further complication is linked to the dense water carried with bottom gravity currents from the Weddell Sea (Killworth, 1977). Furthermore, the vertical density stratification in the Southern Ocean is weak, so small changes in the simulated hydrography in the region may easily result in unrealistic ventilation rates.

The presented sensitivity study shows that if CFCs are included in coupled climate models, first order evaluation of decadal-scale ventilation processes can be based on transects like the WOCE P19 transect along 88°W and the Ajax section along the prime meridian. The inclusion of CFCs in coupled climate models is technically straightforward and computationally cheap, and could therefore be used as an efficient and illuminating test-bed for evaluating the ocean uptake of heat and $CO_2$ on decadal timescales.

***Acknowledgments.*** The study has been supported by the G. C. Rieber Foundations, Norsk Hydro as, the Norwegian Research Council through the RegClim and the Programme of Supercomputing projects, and the project GOSAC (ENV4-CT97-0495) under the EC Environment and Climate Programme. The authors would also like to acknowledge the smooth accessibility of the WOCE observations through the WOCE Data Assembly Center at the Scripps Institution of Oceanography (http://whpo.ucsd.edu/). This is publication No. A54 from the Bjerknes Centre for Climate Research.

## REFERENCES

Anderson, L. G., and E. P. Jones , 1991: The transport of $CO_2$ into Arctic and Antarctic Seas: Similarities and differences in the driving processes. *J. Mar. Syst.*, **2**, 81–95.

Arakawa, A., and V. Lamb , 1977: Computational design of the basic processes of the UCLA General Circulation Model. *Methods Comput. Phys.* **17**, 174–265.

Beismann, J.-O., and R. Redler, 2003: Model simulations of CFC uptake in North Atlantic Deep Water: Effects of parameterizations and grid resolution. *J. Geophys. Res.*, **108**(C5), 3159, doi:10.1029/2001JC001253.

Bleck, R., C. Rooth, D. Hu, and L. T. Smith, 1992: Salinity-driven thermohaline transients in a wind- and thermohaline-forced isopycnic coordinate model of the North Atlantic. *J. Phys. Oceanogr.*, **22**, 1486–1515.

Boutin, J., and J. Etcheto, 1997: Long-term variability of the air-sea $CO_2$ exchange coefficient: Consequences for the $CO_2$ fluxes in the equatorial Pacific Ocean. *Global Biogeochem. Cycles*, **11**, 453–470.

Dixon, K., J. Bullister, R. Gammon, and R. Stouffer, 1996: Examining a coupled climate model using CFC-11 as an ocean tracer. *Geophys. Res. Lett.*, **23**, 1957–1960.

Doney, S. C., and M. W. Hecht, 2002: Antarctic bottom water formation and deep-water chlorofluorocarbon distributions in a global ocean climate model. *J. Phys. Oceanogr.*, **32**, 1642–1666.

Dutay, J., and Coauthors, 2002: Evaluation of ocean model ventilation with CFC-11: Comparison of 13 global ocean models. *Ocean Modelling*, **4**(2), 89–120.

Gao, Y., H. Drange, and M. Bentsen, 2003: Effects of diapycnal and isopycnal mixing on the ventilation of CFCs in the North Atlantic in an isopycnic coordinate OGCM. *Tellus*, **55B**(3), 837–854.

Gargett, A., 1984: Vertical eddy diffusivity in the ocean interior. *J. Marine Res.*, **42**(2), 359–393.

Gaspar, P., 1988: Modeling the seasonal cycle of the upper ocean. *J. Phys. Oceanogr.* **18**, 161–180.

Killworth, P. D., 1977: Mixing on the Weddell Sea continential slope. *Deep-Sea Res.*, **24**, 427–448.

Ledwell, J. R., and A. J. Watson, 1993: Evidence for slow mixing across the pycnocline from an open ocean tracer-release experiment. *Nature*, **364**, 701–703.

Ledwell, J. R., E. Montgomery, K. Polzin, L. Laurent, and R. Schmitt, J. Toole, 2000: Evidence for enhanced mixing over rough topography in the abyssal ocean. *Nature*, **403**, 179–182.

Levitus, S., and T. P. Boyer, 1994: *World Ocean Atlas 1994 Volume 4: Temperature*. NOAA Atlas NESDIS 4, Washington, D.C., USA, 129pp.

Levitus, S., R. Burgett, and T. P. Boyer, 1994: *World Ocean Atlas 1994 Volume 3: Salinity*. NOAA Atlas NESDIS 3, Washington, D.C., USA, 111pp.

McDougall, T., and W. Dewar, 1998: Vertical mixing, cabbeling and thermobaricity in layered models. *J. Phys. Oceanogr.*, **28**, 1458–1480.

Muench, R., L. Padman, S. Howard, E. Fahrbach, 2002: Upper ocean diapycnal mixing in the northwestern Weddell Sea. *Deep-Sea Res.*, **49**, 4843–4861.

Oberhuber, J. M., 1988: An atlas based on the "COADS" data set: The budgets of heat, buoyancy and turbulent kinetic energy at the surface of the global ocean. Tech. Rep. 15, Max-Planck-Inst. fűr Meteorol., Hamburg, Germany.

Oberhuber, J. M., 1993: Simulation of the Atlantic circulation with a coupled sea ice - mixed layer - isopycnal general circulation model, Part I: Model description. *J. Phys. Oceanogr.*, **23**(5), 808–829.

Orr, J., and Coauthors, 2001: Estimates of anthropogenic carbon uptake from four three-dimensional global ocean models. *Global Biogeochem. Cycles*, **15**(1), 43–60.

Orsi, A., G. Johnson, and J. Bullister, 1999: Circulation, mixing, and production of Antarctic Bottom Water. *Prog. Oceanogr.*, **43**, 55–109.

Orsi, A. H., W. M. Smethie Jr., and J. L. Bullister, 2002: On the total input of antarctic waters to the deep ocean: A preliminary estimate from chlorofluorocarbon measurements. *J. Geophys. Res.*, **107**(C8), doi: 10.1029/ 2001JC00976.

Robitaille, D., and A. Weaver, 1995: Validation of subgrid-scale mixing schemes using CFCs in a global ocean model. *Geophys. Res. Lett.*, **22**(21), 2917–2920.

Sloyan, B., and S. Rintoul, 2000: Estimates of area-averaged diapycnal fluxes from basin-scale budgets. *J. Phys. Oceanogr.* **30**, 2320–2341.

Smethie Jr, W. M., R. Fine, A. Putzka, and E. Jones, 2000: Tracing the flow of North Atlantic deep water using chlorofluorocarbons. *J. Geophys. Res.*, **105**(C6), 14297–14323.

Spencer, R., 1993: Global Oceanic Precipitation from the MSU during 1979-91 and comparisons to other Climatologies. *J. Climate*, **6**, 1301–1326.

Sun, S., 1997: Compressibility effects in Miami Isopycnic Coordinate Ocean Model. Ph.D. Dissertation, Univ. of Miami, 138pp.

Toole, J. M., K. L. Polzin, and R. W. Schmitt, 1994: Estimates of diapycnal mixing in the abyssal ocean. *Science*, **264**, 1120–1123.

Walker, S., R. Weiss, and P. Salameh, 2000: Reconstructed histories of the annual mean atmospheric mole fractions for halocarbons CFC-11, CFC-12, CFC-113, and carbon tetrachloride. *J. Geophys. Res.*, **105**(C6), 14285–14296.

Wanninkhof, R., 1992: Relationship between wind speed and gas exchange over the ocean. *J. Geophys. Res.*, **97**(C5), 7373–7382.

Warner, M., and R. Weiss, 1992: Chlorofluoromethanes in South Atlantic Antarctic intermediate water. *Deep-Sea Res.*, **39**, 2053–2075.

Willey, D. A., R. A. Fine, R. E. Sonnerup, J. L. Bullister, W. M. Smethie Jr., and M. J. Warner, 2004: Global oceanic chlorofluorocarbon inventory. *Geophys. Res. Lett.*, **31**, L01303, doi:10.1029/2003GL018816.

Woodruff, S., R. Slutz, and R. Jenne, 1987: A comprehensive ocean-atmosphere data set. *Bull. Amer. Meteor. Soc.*, **68**, 1239–1250.